Translational Oncology 14 (2021) 100960

Contents lists available at ScienceDirect

Translational Oncology

journal homepage: www.elsevier.com/locate/tranon

PRRX1 promotes malignant properties in human osteosarcoma

Ryoji Joko[a,b], Daisuke Yamada[a], Masahiro Nakamura[c], Aki Yoshida[b], Shota Takihira[a,b], Tomoka Takao[a], Ming Lu[a], Kohei Sato[b], Tatsuo Ito[d], Toshiyuki Kunisada[b], Eiji Nakata[b], Toshifumi Ozaki[b], Takeshi Takarada[a,*]

[a] Department of Regenerative Science, Okayama University Graduate School of Medicine, Dentistry and Pharmaceutical Sciences, 2-5-1 Shikata-cho, Kita-ku, Okayama 700-8558, Japan
[b] Department Orthopedic Surgery, Okayama University Graduate School of Medicine, Dentistry and Pharmaceutical Sciences, Okayama 700-8558, Japan
[c] Precision Health, Department of Bioengineering, Graduate School of Engineering, The University of Tokyo, Tokyo 113-8656, Japan
[d] Department of Hygiene, Kawasaki Medical School, Kurashiki, Japan

ARTICLE INFO

Keywords:
PRRX1
Osteosarcoma
Tumor malignancy
Invasion
Drug resistance
Connectivity map analysis

ABSTRACT

Paired related homeobox 1 (PRRX1) is a marker of limb bud mesenchymal cells, and deficiency of p53 or Rb in Prrx1-positive cells induces osteosarcoma in several mouse models. However, the regulatory roles of PRRX1 in human osteosarcoma have not been defined. In this study, we performed PRRX1 immunostaining on 35 human osteosarcoma specimens to assess the correlation between PRRX1 level and overall survival. In patients with osteosarcoma, the expression level of PRRX1 positively correlated with poor prognosis or the ratio of lung metastasis. Additionally, we found PRRX1 expression ~~on~~ in 143B cells, a human osteosarcoma line with a high metastatic capacity. Downregulation of PRRX1 not only suppressed proliferation and invasion but also increased the sensitivity to cisplatin and doxorubicin. When 143B cells were subcutaneously transplanted into nude mice, PRRX1 knockdown decreased tumor sizes and rates of lung metastasis. Interestingly, forskolin, a chemical compound identified by Connectivity Map analysis using RNA expression signatures during PRRX1 knockdown, decreased tumor proliferation and cell migration to the same degree as PRRX1 knockdown. These results demonstrate that PRRX1 promotes tumor malignancy in human osteosarcoma.

Introduction

Osteosarcoma is the most frequent malignant tumor of the bone in the pediatric age group [1]. Metastases are detectable in 15%–20% of patients at initial presentation, mostly in the lungs, and 30%–40% develop lung metastases during or after treatment [2-4]. Despite advances in surgery, chemotherapy, and radiotherapy, prognosis remains poor in patients with metastatic disease with a five-year overall survival rate of 24%–40% [4,5]. Unfortunately, clinical studies, such as those examining targeted agents, have shown disappointing results and changed little in the last three decades [1]. For the development of novel treatments to improve the prognosis of osteosarcoma patients, further elucidation of the molecular mechanisms that support the invasion and proliferation of osteosarcoma cells is of paramount importance [6-10].

Paired related homeobox 1 (PRRX1) is a member of the paired-type family of homeobox transcription factors, which have important functions in the regulation of developmental morphogenetic processes [11-13]. During mouse development, Prrx1 is highly expressed in limb bud mesenchymal or craniofacial-mesenchymal cells, and mice lacking Prrx1 or humans with a PRRX1 mutation die perinatally due to craniofacial and limb malformations [14-16].

Recently, the oncogenic or tumor-suppressive functions of Prrx1 have been reported in several tumors. In glioma and pancreatic cancer, Prrx1 was highly expressed in tumor-initiating cells and displayed a regulatory role in invasion or metastasis [17-19]. In breast, lung, or hepatocellular cancers, PRRX1 inhibits the self-renewal and stem-like properties of tumor-initiating cells [20-22]. In the sarcoma research field, mice eventually develop osteosarcoma with *p53* and *Rb* deficiency in Prrx1-positive cells or osteoblasts [23-26], indicating a critical role for Prrx1-positive cells in osteosarcoma development. However, the oncogenic function of PRRX1 in human osteosarcoma has not been defined.

Here, we examined the correlation between PRRX1 expression level and prognosis in human osteosarcoma patients. We further investigated the oncogenic role of PRRX1 using human osteosarcoma 143B cells.

Abbreviations: PRRX1, paired related homeobox 1; OS, Osteosarcoma.

* Corresponding author.
E-mail address: takarada@okayama-u.ac.jp (T. Takarada).

https://doi.org/10.1016/j.tranon.2020.100960
Received 18 September 2020; Received in revised form 29 October 2020; Accepted 13 November 2020

Material and method

Case selection

A total of 35 previously untreated patients with osteosarcoma who underwent curative surgery at Okayama Hospital from 1994 to 2014 were enrolled in this study. The patients' medical records, including age at diagnosis, gender, tumor size (diameter), local recurrence, metastasis status, and survival time, were obtained. Clinical follow-up was available with a mean follow-up of 91 months (range, 3–287 months). The detailed information is listed in Fig. 1D. Written informed consent was obtained from all participants before this study, and the Okayama Hospital Institutional Review Board approved the use of all human specimens (Approval code; 1908-001).

Immunohistochemistry

To stain for PRRX1, we prepared slides from clinical samples of osteosarcoma. A paraffin block containing the largest tumor tissue of each lesion was selected. Sections (4 μm thickness) from the paraffin block were routinely deparaffinized. The slides were heated for antigen retrieval in 10 mmol/L sodium citrate (pH 6.0) for 10 min. Endogenous peroxidase was quenched with 3% H_2O_2 in methanol for 10 min. After blocking to reduce nonspecific antibody binding, PRRX1-specific antibody (1:200 dilution, NBP2–13,816; Novus Biologicals, Littleton, CO, USA) was reacted with tissue sections overnight at 4 ˚C, followed by three washes with PBS. The sections were reacted with peroxidase-conjugated anti-rabbit IgG (Histofine Simple Stain Max-PO; Nichirei, Tokyo, Japan). Finally, diaminobenzidine (Simple Stain DAB Solution; Nichirei) was applied as a chromogen and counterstained with hematoxylin. Every tumor was scored according to the intensity of the nucleic staining (no staining = 0, weak staining = 1, moderate staining = 2, strong staining = 3), and the extent of stained cells (0%–5% = 0, 6%–25% = 1, 26%–50% = 2, >50% = 3). The final immunoreactive score was determined by totaling the intensity scores with the extent of positivity scores of stained cells, yielding a minimum score of 0 and a maximum of 6.

Cells and cell culture

Five human osteosarcoma cell lines (Saos-2, MG63, HOS, 143B, and U2OS) were purchased from the American Type Culture Collection (ATCC; Manassas, VA, USA) and lentiX293T cell was purchased from Takara Bio (Kusatsu, Shiga, Japan). They were maintained in Dulbecco's modified Eagle's medium (DMEM; Nacalai Tesque, Inc., Kyoto, Japan). All culture media were supplemented with 10% fetal bovine serum (FBS; Hyclone, Victoria, Australia), penicillin (100 U/mL), and streptomycin (100 mg/mL) (NACALAI TESQUE, Inc.) in a humidified atmosphere containing 5% CO_2 at 37 ˚C.

Production of lentivirus

pLKO.1puro, a lentiviral vector plasmid purchased from Addgene (#8453; Watertown, MA, USA), was digested with AgeI and EcoRI and then ligated with annealed primers using Ligation High ver 2 (Takara Bio). The following primers were used: shPRRX1#1 forward 5′-CCG GTG ACA TTT AGG GTA TAA AGA TCT TCA AGA GAG ATC TTT ATA CCC TAA ATG TCT TTT TTG-3′, shPRRX1#1 reverse 5′-AAT TCA AAA AAG ACA TTT AGG GTA TAA AGA TCT CTC TTG AAG ATC TTT ATA CCC TAA ATG TCA-3′; shPRRX1#2 forward 5′-CCG GTG CAG CGA AGG AAT AGG ACA ACT TCA AGA GAG TTG TCC TAT TCC TTC GCT TTT TTG-3′, shPRRX1#2 reverse 5′-AAT TCA AAA AAG CAG CGA AGG AAT AGG ACA ACT CTC TTG AAG TTG TCC TAT TCC TTC GCT GCA-3′. For lentiviral production, pLKO.1 puro constructs were transfected together with packaging vectors, including pMDLg/pRRE, pRSV-Rev, and pMD2.G, to lentiX293T cells using PEI-MAX reagent (Polysciences, Warrington, PA, USA). Culture media were replaced with fresh media 12 h after transfection. Cells were cultured for 48 h, and culture supernatants containing lentivirus were passed through a 0.45 μM PVDF filter (Hawach Scientific, Xi'an, China). Lentivirus solutions were stored at −80 ˚C until use. For lentiviral infection, 143B cells were treated with the lentiviral solution for 24 h. After culturing for another 24 h without lentivirus, cells were treated with 1 μg/mL puromycin (Wako) to select lentivirus-infected cells.

RNA isolation and RT-qPCR

Total RNA was extracted using an RNeasy mini kit (Qiagen, Hilden, Germany), and cDNA was synthesized using M-MLV Reverse Transcriptase (Thermo Fisher Scientific, Waltham, MA, USA) and oligo-dT primers (Sigma-Aldrich, St. Louis, MO, USA). The cDNA was then used as a template for qPCR analysis with gene-specific primers. The following primers were used: *GAPDH* forward 5′-ACA ACT TTG GTA TCG TGG AAG GA-3′, reverse 5′- TCT GGG TGG CAG TGA TG-3′; PRRX1 forward 5′-CGC AGG AAT GAG AGA GCC AT-3′, reverse 5′-GAG CAG GAC GAG GTA CGA TG-3′. qPCR was performed using an AriaMX Real-Time PCR System (Agilent Technologies, Santa Clara, CA, USA). The cycle parameters were as follows: denaturation at 95 ˚C for 30 s, annealing for 30 s at 62 ˚C, and elongation for 30 s at 72 ˚C. The expression level of each gene was calculated using the $2^{-\Delta\Delta Ct}$ method.

Western blotting

Total protein was extracted with a lysis buffer (0.1 M Tris [pH 6.7], 4% SDS), and nuclear fractions were purified with LysoPure Nuclear and Cytoplasmic Extractor Kit (Wako). Proteins were quantified using a BCA protein assay kit (Thermo Fisher) by measuring absorbance at 450 nm using a Multiskan Sky Microplate Spectrophotometer (Thermo Fisher). Proteins (10 μg) were separated using SDS-PAGE and then electrophoretically transferred to 0.45 μm PVDF membranes (Millipore, Burlington, MA, USA), which were blocked with 5% (w/v) skim milk/0.02% (v/v) Tween 20/PBS, and incubated with primary antibodies (diluted 1:2000) overnight at 4 ˚C. After incubation with HRP-conjugated antibodies (diluted 1:5000; GE Healthcare, Chicago, IL, USA), membranes were reacted with ECL Prime (GE Healthcare) to detect signals using an Amersham Imager 600 (Amersham). The following antibodies were used: PRRX1 (Novusbio, NBP2–13,816 (Fig. 2A) / Sigma-Aldrich, HPA051084 (Fig. 2C)), HDAC2 (#2540; Cell Signaling Technology, Danvers, MA, USA), and HRP anti-rabbit IgG (#7074, Cell Signaling Technology).

RNA-sequence analysis

Total RNA was extracted using an RNeasy mini kit (Qiagen), and sequencing libraries were prepared using a KAPA RNA HyperPrep Kit with RiboErase (HMR) (Kapa Biosystems) and a SeqCap Adapter Kit (Set A or Set B, Roche) following the manufacturer's instructions. Sequencing libraries were transferred to a GENEWIZ (Suzhou, China) and were loaded onto a HiSeq 2500 system (Illumina) for sequencing. All sequence reads were extracted in FASTQ format using the CASAVA 1.8.4 pipeline. Trimmomatic (version 0.36) was used to remove adapters and filter raw reads of < 36 bases in addition to leading and trailing bases of less than quality 20. Filtered reads were mapped to hg19 using HISAT2 (v2.1.0). Raw counts for each gene were based on sense-strand data obtained using featureCounts software from the Subread package. RUVSeq (Release 3.10) was used for further normalization to account for sample variations. Differentially expressed genes were identified through DESeq2 analysis with a threshold of padj < 0.01 and abs (Log_2FC) > 1. The raw and processed RNA-Seq data were deposited in the NCBI GEO database under accession number GSE160296. All sequence data were submitted to GSEA4.0.3 software, and gene sets enrichment analysis (GSEA) was performed.

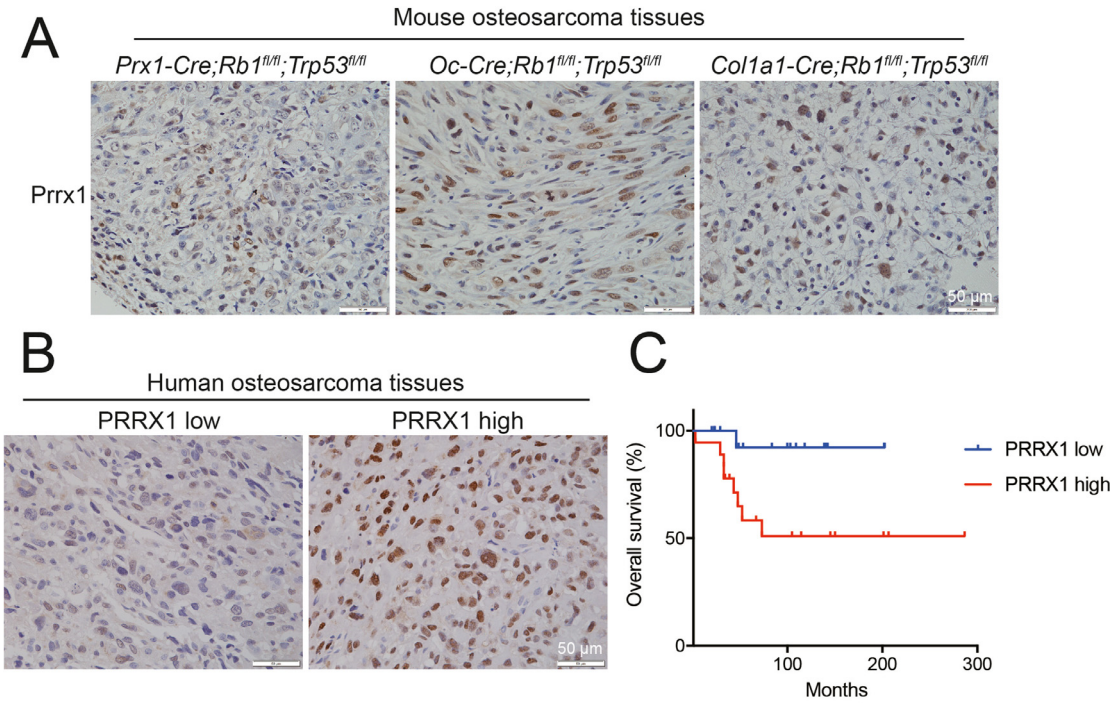

D

Variables	n	PRRX1 expression		P value
		Positive	Negative	
Age, year				
＜18	21	13 (62 %)	8 (38 %)	0.176
≧18	14	5 (36 %)	9 (64 %)	
Gender				
Male	19	9 (47 %)	10 (53 %)	0.738
Female	16	9 (56 %)	7 (44 %)	
Tumor size (cm)				
＜ 8	12	4 (33 %)	8 (67 %)	0.164
≧ 8	23	14 (61 %)	9 (39 %)	
Local recurrence				
+	3	3 (100 %)	0 (0 %)	0.229
-	32	15 (47 %)	17 (53 %)	
Lung metastasis				
+	14	12 (86 %)	2 (14 %)	0.002
-	21	6 (29 %)	15 (71 %)	
Survival time				
＜ 5	9	8 (89 %)	1 (11 %)	0.009
≧ 5	26	10 (38 %)	16 (62 %)	

Fig. 1. Expression of PRRX1 in mouse or human osteosarcoma tissues.
(A) Immunostaining of Prrx1 in mouse osteosarcoma tissues. Sections derived from *Prrx1-Cre;Rb$^{fl/fl}$;Trp53$^{fl/fl}$*, *Oc-Cre;Rb$^{fl/fl}$;Trp53$^{fl/fl}$* or *Col1a1-Cre;Rb$^{fl/fl}$;Trp53$^{fl/fl}$* osteosarcomas were stained with Prrx1 and representative photos are shown. (B) Immunostaining of PRRX1 in human osteosarcoma tissues. Sections derived from human osteosarcomas were stained with PRRX1, and representative photos of PRRX1-low or PRRX1-high tumors are shown. (C) Comparison of overall survival between PRRX1-low and PRRX1-high osteosarcoma patients. Kaplan–Meyer survival curve demonstrates significant (log-rank test, $p < 0.01$) worse overall prognosis for osteosarcoma patients with high expression levels of PRRX1 compared with the PRRX1-low expression group. (D) Correlation of PRRX1 levels with patient clinical and pathological characteristics.

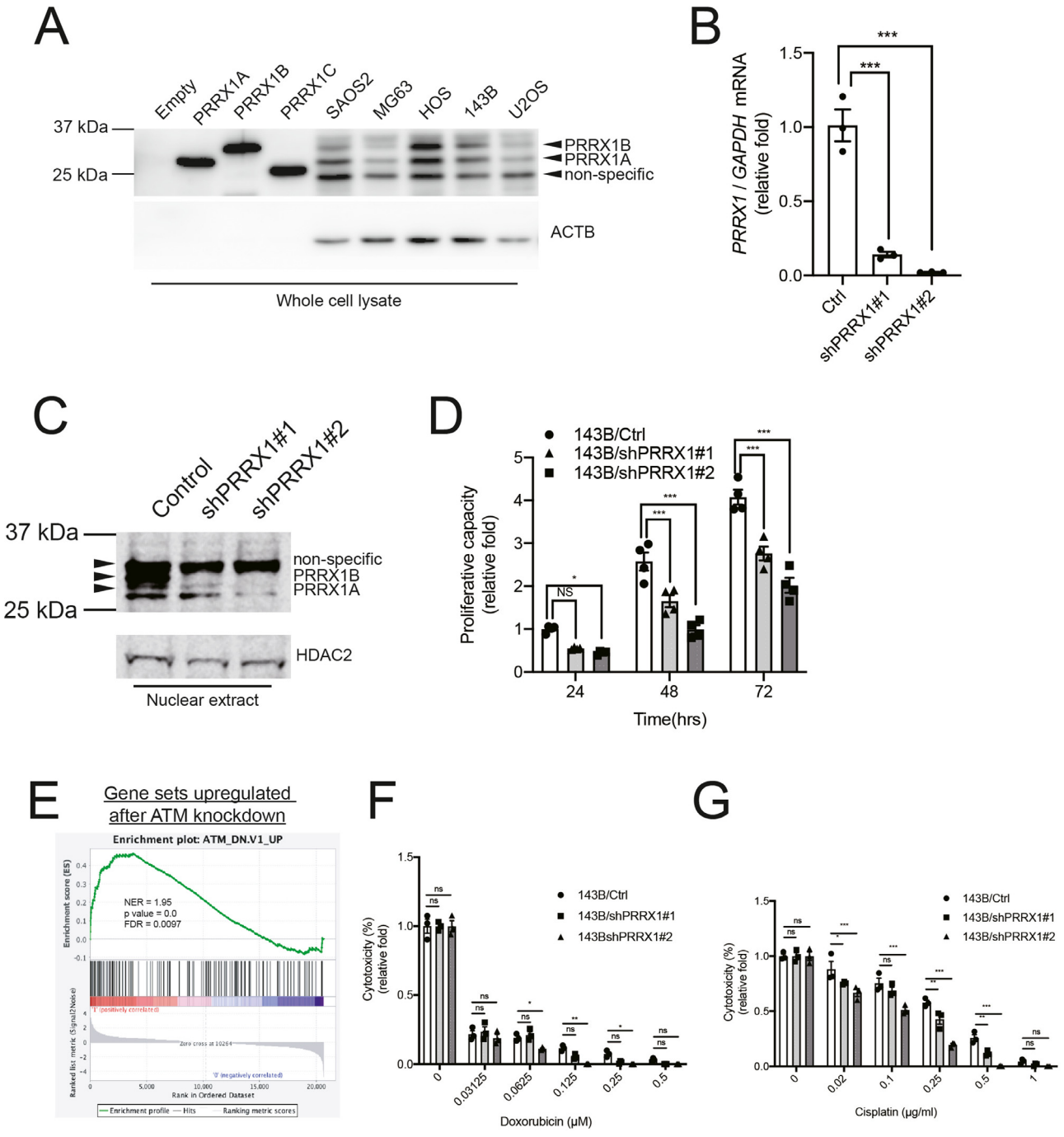

Fig. 2. Effects of PRRX1 knockdown on proliferative capacity or drug sensitivity of human osteosarcoma cells.
(A) Detection of PRRX1 in human osteosarcoma cell lines by western blot analysis. Total protein was extracted from the human osteosarcoma cell lines SAOS2, MG63, HOS, 143B, and U2OS, and the expression of PRRX1 in each was assessed compared with cell lysates prepared from HEK293T cells overexpressing each PRRX1 isoform as reference. (B) RT-qPCR analysis of *PRRX1* in 143B cells after PRRX1 knockdown. The 143B cells were infected with a lentivirus encoding each shPRRX1 clone, and total RNA was extracted to compare the expression level of *PRRX1* mRNA. All values were normalized to *GAPDH* mRNA level ($n = 3$) (C) Western blot analysis after PRRX1 knockdown. The 143B cells were infected with lentivirus encoding each shPRRX1 clone, and nuclear lysates were extracted to compare the expression level of PRRX1. (D) Comparison of proliferative capacity by WST-1 assay. The 143B/Ctrl or 143B/shPRRX1#1 or #2 cells were seeded in a 96-well plate, and the OD_{450} was measured at each indicated time point ($n = 4$, two independent experiments). (E) Comparison of the RNA transcriptome after PRRX1 knockdown. RNA-seq of 143B/Ctrl and 143B/shPRRX1#2 was performed, and data were compared by gene sets enrichment analysis (GSEA). Genes upregulated in 143B/shPRRX1#2 were clustered at the left ($n = 2$, two independent experiments). (F, G) Comparison of cisplatin (F) or doxorubicin (G) sensitivity after PRRX1 knockdown. Cells were treated with cisplatin or doxorubicin for 72 h, and the ratio of living cells was assessed by WST-1 assay. The ratio of DMSO-treated cells was set to 100% ($n = 3$, two independent experiments).

For Connectivity Map analysis, we obtained two sets of lists with 68 upregulated and 73 downregulated genes after PRRX1 knockdown to identify overexpressed or underexpressed signatures, respectively. The two gene lists were queried through the L1000-Query tool interface in the CMap project (https://www.broadinstitute.org/connectivity-map-cmap). The L1000-Query tool includes the CMap reference dataset, which contains a subset of profiles derived from 8388 tested perturbagens (2429 of which are compounds), known as the TouchstoneV1.1 dataset. The compound ranking results with signature similarity scores were exported.

Cell proliferation assay

Cells were plated on 96-well plates at 1×10^3 cells per well in a final volume of 100 μL per well. Cell viability was determined using cell proliferation reagent WST-1 (Sigma-Aldrich) according to the manufacturer's protocol. For comparison of proliferative capacity, cells were cultured for 24, 48, or 72 h. For the cytotoxicity assay, cells were treated with each indicated dose of doxorubicin (Sigma-Aldrich) or cisplatin (Enzo Life Sciences, Farmingdale, NY) for 72 h. WST-1 substrate (10 μL) was added to each well and incubated for 2 h at 37 ˚C in 5% CO_2. Absorbance at 450 nm was measured using a microplate reader (Bio-Rad). Each experiment was performed in triplicate.

Wound healing assay

A scratch wound healing assay was used to examine cell mobility characteristics. Briefly, 143B/Ctrl or 143B/shPRRX1 cells (1.2×10^5 cells/well) were grown in a 24-well plate until confluency. The medium was replaced with serum-free DMEM. Cell monolayers were scratched (wounded) using a sterile 200 μL pipette tip, and PBS was used for washing and removing cell debris. After 16 h, migrating cells were monitored and photographed under phase-contrast microscopy. Image J software was used to quantify the relative wound size. Cell mobility inhibition (%) was calculated as the new scratch width / original scratch width × 100%. Experiments were repeated three times.

Transwell assay

Cell invasion and migration were examined with 24-well BD BioCoat invasion chambers. Matrigel matrix (BD Biosciences, San Jose, CA, USA) was used for invasion assay. A total of 2×10^5 cells were suspended in 500 μL DMEM without FBS and added to the upper chamber. DMEM with 10% FBS was added to the lower chamber. After incubation for 16 h, the cells on the upper surface of the filter were completely removed by wiping with cotton swabs. The filters were fixed in methanol and stained with Hemacolor® solution 3 (Merck, Darmstadt, Germany). The filters were then mounted onto slides, and the cells on the lower surfaces were counted in six randomized high-power fields.

Measurement of PKA activity

PKA activity was measured with PKA Kinase Activity Assay Kit (abcam) followed by manufacuture's instruction. For 143B/Ctrl, 143B/shPRRX1#1 and 143B/shPRRX1#2, cell lysates were prepared when cells reached at 80% confluency. For forskolin treatment, cells were treated with 0.1, 1 or 10 μM forskolin for 24 hr and then cell lysates were prepared. Absorbance at 450 nm was measured using a microplate reader (Bio-Rad) and all values were normalized to total protein level.

Xenograft models

The Okayama University Animal Care and Use Committee approved the experiments using mice and animal care procedures. Four-week-old female BALB/c nude mice were purchased from Japan SLC (Shizuoka, Japan). On day 0, the mice were anesthetized with 3% isoflurane, and 100 μL containing 2.0×10^7 cells of 143B/Ctrl ($n = 5$), 143B/shPRRX1, ($n = 5$) cells was injected into the left flank. The volumes of tumors were calculated using the formula: $L \times W^2 \times 0.5$, where L is the length, and W is the width of each tumor, as reported previously [27]. For evaluation of lung metastases, mice were sacrificed, and lungs were removed and sliced (2 mm). H&E staining of the extracted lung tissue and immunostaining of PRRX1 (Novusbio) were performed, and the number of lung metastases was counted by two observers. Ki-67 (ab16667; Abcam, Cambridge, MA, USA), and terminal dUTP nick-end labeling (TUNEL) staining (Sigma-Aldrich) were also performed [28].

Statistical analysis

Data analysis was performed using Prism 8 (GraphPad Software, San Diego, CA, USA). All data were acquired by performing biological replicas of two or three independent experiments and are presented as the means ± SEM. Statistical significance was determined using a two-tailed *t*-test and unpaired one-way or two-way ANOVA with Tukey's post hoc analysis.

Results

PRRX1 level positively correlated with poor prognosis of patients with human osteosarcoma

Although Jones et al. reported that p53 and Rb deletion in *Prrx1, Osteocalcin* (*Oc*), or *Col1α1*-positive cells induces the formation of osteosarcoma [26], the expression of Prrx1 in each developed tumor has not been investigated. When tissue sections derived from such osteosarcomas were assessed by immunohistological staining, all tumors were Prrx1 positive (Fig. 1A). We also found that all 35 human osteosarcoma patients in our study expressed PRRX1 and could be subdivided into a high-expression group ($n = 18$, 51%) or a low-expression group ($n = 17$, 49%) based on our criteria (Fig. 1B). Interestingly, the expression level of PRRX1 was significantly associated with five-year overall survival (high *vs.* low: 58% *vs.* 92%, $P < 0.05$; Fig. 1C). Fig. 1D shows the correlation between PRRX1 level and clinicopathological parameters of osteosarcoma. The mean tumor size was 10.1 cm (range, 3.0–21.0 cm). The PRRX1 expression level was compared between patients with or without lung metastasis, and PRRX1-high patients were more frequently found in the lung metastasis group (85.7% *vs.* 28.6%, $P < 0.01$). Also, the PRRX1 expression level was significantly higher in patients surviving fewer than five years than those surviving for more than five years. No significant correlation was observed between PRRX1 level and age, gender, tumor size, or local disease recurrence. These results demonstrate that PRRX1 serves as a malignant factor in human osteosarcoma.

PRRX1 knockdown decreased cell proliferation and drug sensitivity in human osteosarcoma

To investigate the function of PRRX1 in human osteosarcoma, we tested its expression by western blot analysis in several human osteosarcoma cell lines (SaOS-2, MG63, HOS, 143B, and U2OS) (Fig. 2A). PRRX1 has three isoforms, and these were used as a reference. Although all cell lines expressed PRRX1A or PRRX1B, HOS or 143B cells expressed higher levels than the other lines. Thus, we chose 143B for further experiments because of its high metastatic capacity or malignancy [29]. To suppress the function of PRRX1, we designed two shRNA sequences against PRRX1 (shPRRX1) and recombined them into a lentiviral vector, pLKO1.puro. After introducing control or each shPRRX1 to 143B cells via lentiviral infection, cells were selected with puromycin, and PRRX1 level was compared at the mRNA or protein level (Fig. 2B, C). We found that both PRRX1A and PRRX1B were downregulated by PRRX1 knockdown (Fig. 2C). Hereafter, 143B cells infected with control, shPRRX1#1,

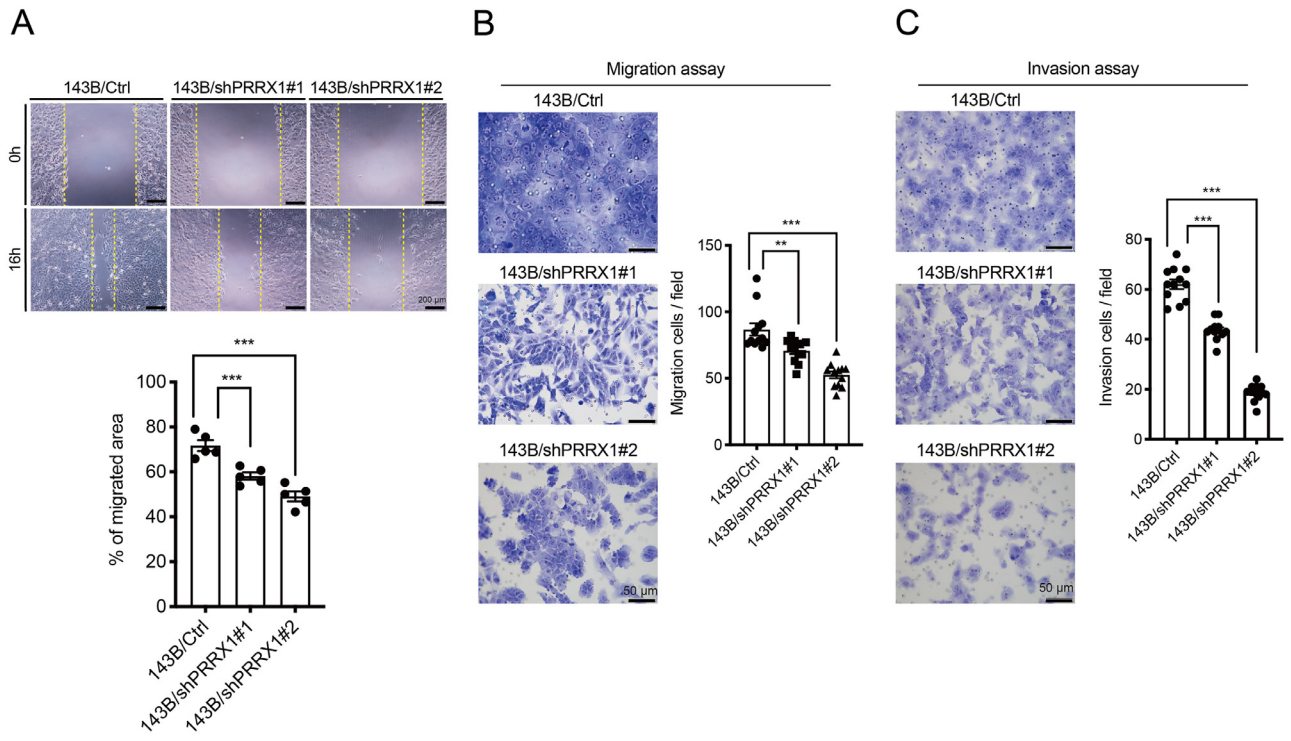

Fig. 3. Effects of PRRX1 knockdown on migration or invasion of human osteosarcoma cells.
(A, B) Comparison of migration capacity after PRRX1 knockdown by wound healing assay (A) or migration assay (B). For the wound-healing assay, the relative migration of 143B/shPRRX1#1 or #2 cells was lower than that of 143B/Ctrl at 16 h after scratch wound ($n = 5$, two independent experiments). For the migration assay, transwell plates were used to assess migration. The number of migrated cells was significantly decreased in 143B/shPRRX1#1 or #2 ($n = 12$, two independent experiments). (C) Comparison of invasion capacity after PRRX1 knockdown by invasion assay. Transwell plates were used to assess the invasion. The number of migrated cells was significantly decreased in 143B/shPRRX1#1 or #2 ($n = 12$, two independent experiments).

or #2 lentiviruses are referred to as 143B/Ctrl, 143B/shPRRX1#1, or 143B/shPRRX1#2, respectively.

To compare cell proliferation after PRRX1 knockdown, we performed WST-1 assay and found that 143B/shPRRX1#1 or #2 cells showed lower NADPH-reducing activity than 143B/Ctrl cells at 48 or 72 h after seeding (Fig. 2D). Inhibitory effect of PRRX1 knockdown on proliferation was also tested using another human OS line, HOS (Supplemental Fig. 2). For systematic analysis of the effect of PRRX1 knockdown on the RNA transcriptome of 143B cells, RNA was extracted from each cell line, and RNA-seq or GSEA analysis was performed. As shown in Fig. 2E, gene sets upregulated after knockdown of the ataxia-telangiectasia mutated (ATM) gene were significantly increased by PRRX1 knockdown. Cisplatin or doxorubicin are clinically used chemotherapeutics to treat osteosarcomas, and ATM knockdown increases the sensitivity to these drugs when combined with p53 deficiency [30,31]. As 143B cells are p53-null [32], we compared the sensitivity to these drugs by WST-1 assay. The ratio of living cells was lower in 143B/shPRRX1#1 or 143B/shPRRX1#2 cells, indicating that PRRX1 knockdown increased the sensitivity to doxorubicin and cisplatin (Fig. 2F, G). These results demonstrate that PRRX1 promotes cell proliferation and drug resistance in human osteosarcoma cells.

PRRX1 knockdown decreased migration or invasion in human osteosarcoma

Next, we assessed the effect of PRRX1 knockdown on migration or invasion in human osteosarcoma by wound healing or migration assay. Confluent cells were scratched, and migrated areas were compared after 16 h. Although there were no differences in cell morphology (Supplemental Fig. 2), 143B/shPRRX1#1 or #2 cells displayed lower migration activity than 143B/Ctrl cells (Fig. 3A). The migration assay also provided the same results (Fig. 3B). When invasive capacities were compared by invasion assay, we found that PRRX1 knockdown significantly decreased the invasive capacity of 143B cells (Fig. 3C). These results demonstrate that PRRX1 promotes migration and invasion in human osteosarcoma cells.

PRRX1 knockdown suppressed osteosarcoma development in a mouse xenograft model

To determine the effect of PRRX1 knockdown on osteosarcoma development, we performed a xenograft transplantation assay. The 143B/Ctrl or 143B/shPRRX1#2 cells were subcutaneously transplanted into the left flank of nude mice, and the volumes of the developing tumors were measured at each indicated time point. As shown in Fig. 4A, 143B/shPRRX1#2 formed smaller tumors than 143B/Ctrl. Tumors were excised at 21 days after transplantation, and tumors formed by 143B/shPRRX1#2 cells had lower weights (Fig. 4B). Additionally, tumors derived from 143B/shPRRX1#2 cells showed lower expression levels of PRRX1 and Ki-67 (Fig. 4C, D). The apoptotic ratio assessed by TUNEL assay found no significant differences (Fig. 4C, E). The lung metastatic ratio was compared by counting PRRX1-positive nodules in lung sections, and fewer PRRX1-positive metastases were found in the 143B/shPRRX1#2-transplanted group (Fig. 4F). These results demonstrate that PRRX1 promotes tumor growth and metastasis in human osteosarcoma cells.

Identification of forskolin as a chemical compound that induces the same RNA expression signatures as PRRX1 knockdown in human osteosarcoma cells

RNA-seq analysis revealed that PRRX1 knockdown induced the upregulation of 68 genes and downregulation of 73 genes (Fig. 5A and Supplemental Table 1). Connectivity Map is a useful approach to match

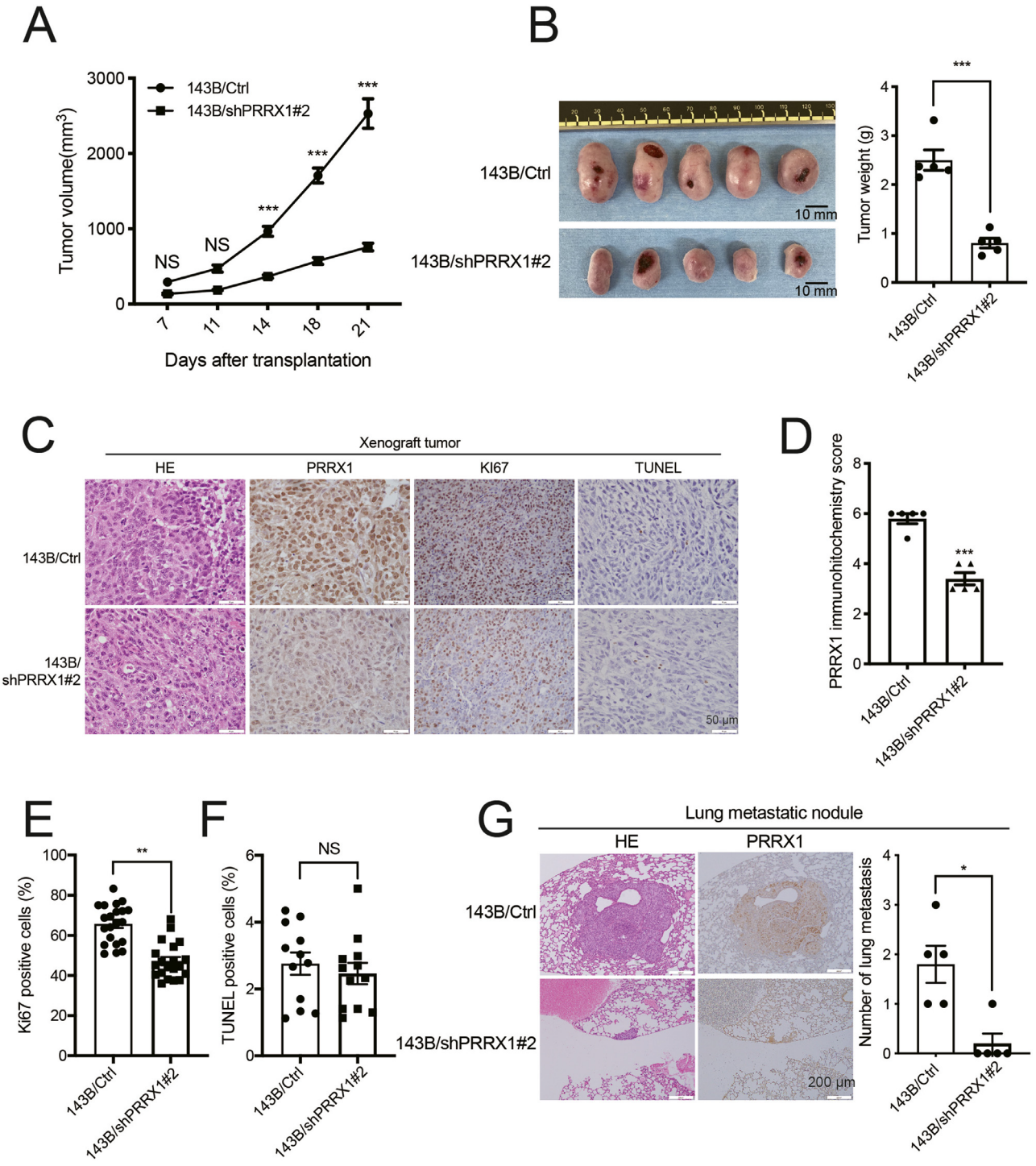

Fig. 4. Effects of PRRX1 knockdown on tumor growth.

(A) Comparison of tumor volume after PRRX1 knockdown. The 143B/Ctrl or 143B/shPRRX1#2 cells were subcutaneously transplanted into nude mice, and the tumor volume at each indicated time point was measured (A). At 21 days after transplantation, mice were sacrificed, and the weights of the developed tumors were measured (B) ($n = 5$, two independent experiments). (C) Immunohistological analysis of developed xenograft tumors derived from 143B/Ctrl or 143B/shPRRX1#2 cells. Tumor sections were stained with hematoxylin and eosin (H&E), immunostained for PRRX1 or Ki-67, or stained by TUNEL. Representative photomicrographs are shown. (D, E, F) Quantification of Ki-67- or TUNEL-positive cells in tumors developed from each cell line. Two or three fields in each tumor section were assessed, and the intensity of PRRX1 (D) or the numbers of cells positive for Ki-67 (D) or TUNEL (E) were compared ($n = 5$). (G) Comparison of lung metastasis after PRRX1 knockdown. Lung tissues were harvested 21 days after transplantation, and PRRX1-positive metastatic nodules were quantified. Tissue sections were sampled at 1 mm intervals, and the number of metastatic nodules in each section was added together ($n = 5$).

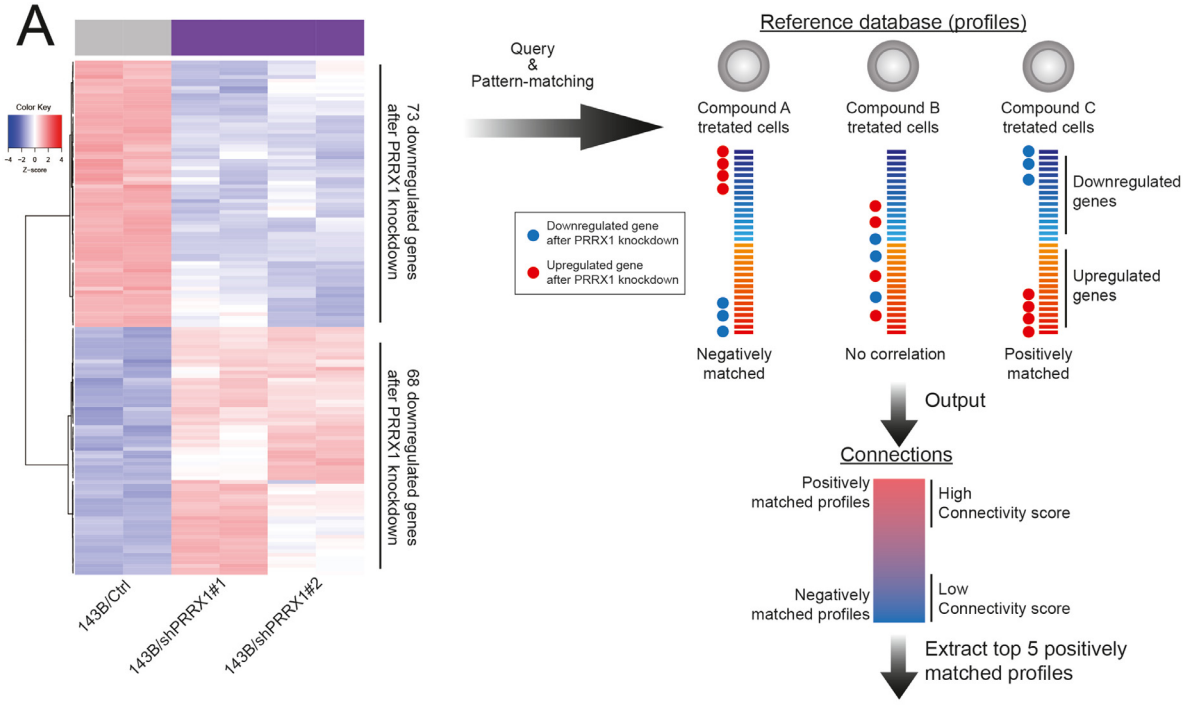

Score of each cell line

Rank	Chemical name	PC3	VCAP	A375	A549	HA1E	HCC515	HT29	MCF7	HEPG2	summary
1	forskolin	93.63	0.00	0.00	88.98	0.00	86.93	98.01	87.93	0.00	93.08
2	scopolamine	85.33	-62.68	80.48	-56.28	91.98	-71.36	0.00	-68.84	76.50	79.17
3	BMY-45778	73.79	99.82	-48.20	85.99	0.00	0.00	0.00	71.96	#N/A	79.12
4	lasalocid	0	87.19	74.87	31.37	57.44	0.00	0.00	81.79	81.34	74.95
5	puromycin	53.91	62.21	0.00	94.86	0.00	-33.21	78.43	0.00	73.04	72.55

*0 indicates no correlation.
N/A means not analyzed.

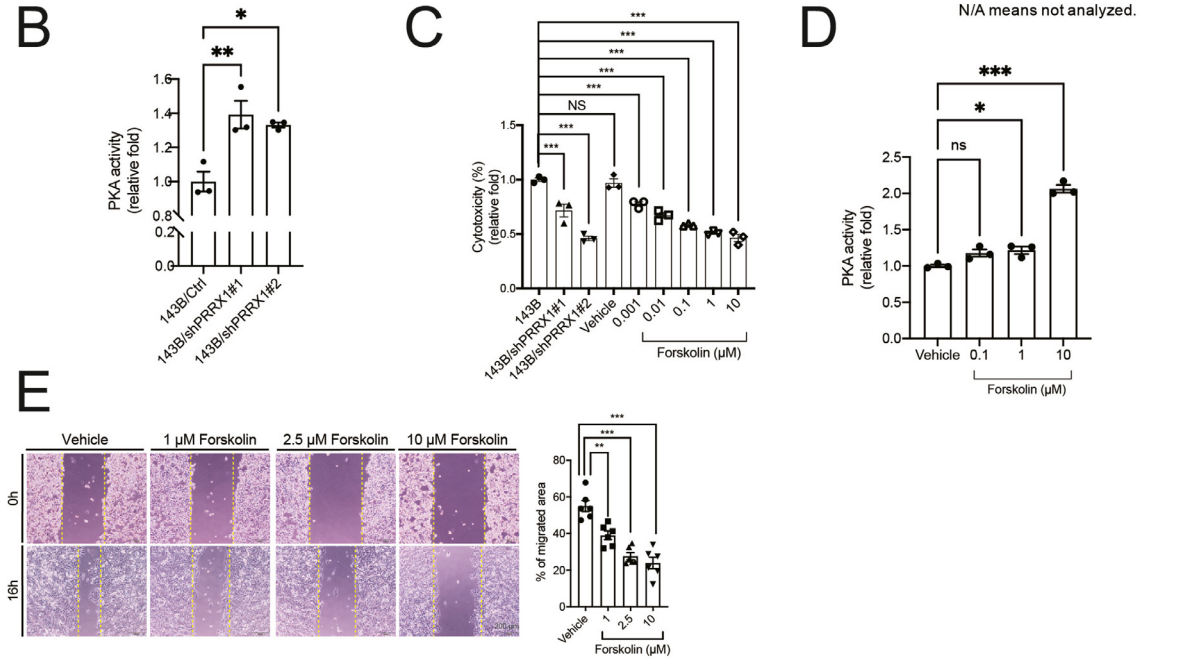

Fig. 5. Identification of forskolin as a chemical compound that induces the same RNA expression signatures as those for PRRX1 knockdown in human osteosarcoma cells.

(A) Schematic demonstrating how to perform Connectivity Map analysis. The 73 downregulated or 68 upregulated genes after PRRX1 knockdown ($n = 2$, two independent experiments) were submitted to the reference database, and pattern-matching was performed. Chemical names listed in the top five positively matched profiles are shown (table in the lower panel). (B) PKA activity after PRRX1 knockdown. ($n = 3$, two independent experiments) (C) The effect of forskolin treatment on the proliferative capacity of 143B cells. The 143B cells were treated with indicated doses of forskolin for 72 h, and cytotoxicity was evaluated via WST-8 assay ($n = 5$, two independent experiments). (D) PKA activity after forskolin treatment. Cell were treated with each indicated concentration of forkolin for 24 h and thne PKA activities were compared. ($n = 3$, two independent experiments) (E) Comparison of migration capacity after forskolin treatment by a wound-healing assay. The relative migration of forskolin-treated cells was lower than that of the vehicle-treated cells (0.1% DMSO) at 16 h after scratching ($n = 5$, two independent experiments).

changes in gene expression for disease indications or drug responses [33-35]. The CMap database contains over one million gene expression signatures from the treatment of a variety of cell types with perturbagens that span a range of small-molecule compounds and gene-overexpression or gene-knockdown agents. Interestingly, when these upregulated or downregulated genes were used for Connectivity Map analysis, we found that the RNA transcriptome of 143B approached that of forskolin-treated cells after PRRX1 knockdown, suggesting that forskolin may decrease the proliferation of 143B. Increases in PKA activity after PRRX1 knockdown was confirmed by ELISA analysis (Fig. 5B). Indeed, treatment with forskolin decreased the NADPH-reducing activity or proliferative capacity of 143B cells as similar to PRRX1 knockdown (Fig. 5C). As PKA activity was significantly increased by forskolin at more than 1 μM (Fig. 5D), we tested the inhibitory effect of 1 μM, 2.5 μM or 10 μM forskolin on the migration activity of 143B cells (Fig. 5E). These results suggest that forskolin confers the same phenotypes that were induced by PRRX1 knockdown in human osteosarcoma cells.

Discussion

Here, the clinical study of sarcoma patients demonstrated that PRRX1 was overly expressed in human osteosarcomas. During the developmental process of the limb bud, PRRX1-positive limb bud mesenchymal (LBM) cells originate from lateral plate mesoderm (LPM) [36] and eventually differentiate into chondrocytes or osteoblasts in limb bones [37]. Mice with a deficiency of *p53* and *Rb1* in Prrx1-positive LBM cells and Col1a1- or osteocalcin-positive osteoblasts develop osteosarcomas [26] that are strongly stained with PRRX1 (Fig. 1A–C). These results suggest that osteoblasts may have acquired LBM-like properties during the process of transformation from normal cells to osteosarcoma cells. Several drugs show anti-tumorigenic effects by inducing the differentiation of cancer cells [38], suggesting that novel therapeutic strategies against osteosarcoma may be developed by understanding the differentiation process from LBM cells to osteoblasts. Thus, further studies are warranted to reveal the detailed mechanism of osteogenic differentiation from human LBM cells.

Several groups have reported that PRRX1 is expressed in stem/progenitor-like cells, and its deficiency decreases their proliferation [18,39]. The proliferative capacity and tumor growth of human osteosarcoma cell lines were decreased by PRRX1 knockdown (Figs. 2D and 4), indicating that PRRX1 also promotes tumor development in osteosarcoma by increasing cell proliferation. Additionally, PRRX1 can bind to the promoter region of several cytokines that are related to tumorigenesis [18], suggesting that PRRX1 may regulate the development of osteosarcoma by modulating its surrounding microenvironment. Although we have no critical data about the isoform-specific function of PRRX1 in osteosarcoma, they may have different roles as previously reported [17,18].

During tumor metastasis, tumor cells must acquire an epithelial-like state to increase their invasiveness via epithelial-to-mesenchymal transition (EMT) [18,21,40-42]. As reported for glioblastoma or pancreatic cancer [18,19], PRRX1 knockdown decreased the migration or invasion capacity of 143B cells (Fig. 3). Osteoblasts reside in bone tissue to produce bone matrix, but LBM cells, Prrx1-positive precursors for osteoblasts, migrate or invade in developing limb to produce chondrocytes or osteoblasts [37]. If PRRX1 promotes the dedifferentiation of osteoblasts to LBM-like cells or to a highly invasive state, the inhibition of PRRX1 in osteosarcoma cells may suppress their invasive capacity by inducing differentiation into osteoblasts.

Tumor cells often show drug resistance via such mechanisms as genomic mutations, activation of the bypass pathway, drug transporters, or the tumor microenvironment [38]. We found that PRRX1 knockdown in 143B cells increased their sensitivity to cisplatin and doxorubicin (Fig. 2F, G). Additionally, RNA transcriptome analysis revealed that PRRX1 knockdown upregulated gene sets associated with the ATM knockdown phenotype (Fig. 2F). Cisplatin and doxorubicin cause DNA damage to kill cells [43,44], and the suppression of ATM activity in p53-deficient cells increases sensitivity to these drugs [31]. These results demonstrate that the inhibition of PRRX1 in 143B (P53-null [32]) cells decreased the activity of ATM and sensitized cells to cisplatin and doxorubicin. Interestingly, Connectivity Map analysis revealed that PRRX1 knockdown produced the same RNA expression signature as that of forskolin treatment (Fig. 5A). Forskolin, an activator of protein kinase A (PKA) signaling, decreased the proliferation and migration of 143B cells (Fig. 5B, C), suggesting that PRRX1 may promote tumor malignancy by suppressing PKA signaling in human osteosarcoma. Furthermore, our RNA transcriptome data also revealed that PRRX1 knockdown decreased the expression level of *S1PR1* that has been reported to be a critical molecule for metastasis [45-47]. Althogh we did not assessed the functional relationship between S1PR1 and PRRX1 in this study, this may be a critical factor to cause the malignancy of osteosarcoma.

Taken together, our results demonstrate that PRRX1 serves as a malignant factor in osteosarcoma by promoting tumor growth, invasion, and drug resistance. We expect that the discovery or development of PRRX1 inhibitors will improve current therapeutic strategies against osteosarcoma and improve our understanding of the pathophysiological roles of PRRX1 in various types of cancer.

Author contributions

R.Joko., D.Yamada. performed the experiments, analyzed the data and wrote the manuscript. M.Nakamura., A.Yoshida., S.Takihira., To. Takao., M.Lu., K.Sato. performed the experiments. T.Ito., E.Nakata., T.Kunisada., T.Ozaki. and Ta.Takarada. discussed the data and provided critical advice. Ta.T.* supervised the project and wrote the manuscript.

Declaration of Competing Interest

The authors declare no competing interests.

Acknowledgments

We thank Dr. Jones, K. B. for providing the paraffin-embedded tissue samples of mouse osteosarcoma. Preparation of slides and staining was supported by Central Research Laboratory, Okayama University Medical School. We thank the members of the Department of Animal Resources, Advanced Science Research Center, and Okayama University for maintaining the mice. This research was supported by Grants-in-Aid for Scientific Research from the Japan Society for the Promotion of Science to D.Y. (no. 18K15212) and E.N. (no. 19K09551), AMED under Grant Number JP19lm0203008. These funders had no role in the study design, data collection and analysis, decision to publish, or preparation of the manuscript.

Supplementary materials

Supplementary material associated with this article can be found, in the online version, at doi:10.1016/j.tranon.2020.100960.

References

[1] Y. Zhang, J. Yang, N. Zhao, C. Wang, S. Kamar, Y. Zhou, Z. He, J. Yang, B. Sun, X. Shi, L. Han, Z. Yang, Progress in the chemotherapeutic treatment of osteosarcoma, Oncol. Lett. 16 (2018) 6228–6237.
[2] N. Vijayamurugan, S. Bakhshi, Review of management issues in relapsed osteosarcoma, Expert Rev. Anticancer Ther. 14 (2014) 151–161.
[3] C. Meazza, P. Scanagatta, Metastatic osteosarcoma: a challenging multidisciplinary treatment, Expert Rev. Anticancer Ther. 16 (2016) 543–556.

[4] B. Kempf-Bielack, S.S. Bielack, H. Jürgens, D. Branscheid, W.E. Berdel, G.U. Exner, U. Göbel, K. Helmke, G. Jundt, H. Kabisch, M. Kevric, T. Klingebiel, R. Kotz, R. Maas, R. Schwarz, M. Semik, J. Treuner, A. Zoubek, K. Winkler, Osteosarcoma relapse after combined modality therapy: an analysis of unselected patients in the cooperative osteosarcoma study group (COSS), J. Clin. Oncol. 23 (2005) 559–568.

[5] A.J. Chou, E.S. Kleinerman, M.D. Krailo, Z. Chen, D.L. Betcher, J.H. Healey, E.U. Conrad, M.L. Nieder 3rd, M.A. Weiner, R.J. Wells, R.B. Womer, P.A. Meyers, Addition of muramyl tripeptide to chemotherapy for patients with newly diagnosed metastatic osteosarcoma: a report from the children's oncology group, Cancer 115 (2009) 5339–5348.

[6] A.J. Saraf, J.M. Fenger, R.D. Roberts, Osteosarcoma: accelerating progress makes for a hopeful future, Front. Oncol. 8 (2018) 4.

[7] T.M. Fan, R.D. Roberts, M.M. Lizardo, Understanding and modeling metastasis biology to improve therapeutic strategies for combating osteosarcoma progression, Front. Oncol. 10 (2020) 13.

[8] K.H. Lu, C.W. Lin, Y.H. Hsieh, S.C. Su, R.J. Reiter, S.F. Yang, New insights into antimetastatic signaling pathways of melatonin in skeletomuscular sarcoma of childhood and adolescence, Cancer Metastasis Rev. 39 (2020) 303–320.

[9] B. Otoukesh, B. Boddouhi, M. Moghtadaei, P. Kaghazian, M. Kaghazian, Novel molecular insights and new therapeutic strategies in osteosarcoma, Cancer Cell Int. 18 (2018) 158.

[10] M. Ehnman, W. Chaabane, F. Haglund, P. Tsagkozis, The tumor microenvironment of pediatric sarcoma: mesenchymal mechanisms regulating cell migration and metastasis, Curr. Oncol. Rep. 21 (2019) 90.

[11] P. Cserjesi, B. Lilly, L. Bryson, Y. Wang, D.A. Sassoon, E.N. Olson, MHox: a mesodermally restricted homeodomain protein that binds an essential site in the muscle creatine kinase enhancer, Development 115 (1992) 1087–1101.

[12] T. Takarada, R. Nakazato, A. Tsuchikane, K. Fujikawa, T. Iezaki, Y. Yoneda, E. Hinoi, Genetic analysis of Runx2 function during intramembranous ossification, Development 143 (2016) 211–218.

[13] K.M. Loh, A. Chen, P.W. Koh, T.Z. Deng, R. Sinha, J.M. Tsai, A.A. Barkal, K.Y. Shen, R. Jain, R.M. Morganti, N. Shyh-Chang, N.B. Fernhoff, B.M. George, G. Wernig, R.E. Salomon, Z. Chen, H. Vogel, J.A. Epstein, A. Kundaje, W.S. Talbot, P.A. Beachy, L.T. Ang, I.L. Weissman, Mapping the pairwise choices leading from pluripotency to human bone, heart, and other mesoderm cell types, Cell 166 (2016) 451–467.

[14] J.F. Martin, A. Bradley, E.N. Olson, The paired-like homeo box gene MHox is required for early events of skeletogenesis in multiple lineages, Genes Dev. 9 (1995) 1237–1249.

[15] D. ten Berge, A. Brouwer, J. Korving, M.J. Reijnen, E.J. van Raaij, F. Verbeek, W. Gaffield, F. Meijlink, Prx1 and Prx2 are upstream regulators of sonic hedgehog and control cell proliferation during mandibular arch morphogenesis, Development 128 (2001) 2929–2938.

[16] M. Dasouki, B. Andrews, P. Parimi, D. Kamnasaran, Recurrent agnathia-otocephaly caused by DNA replication slippage in PRRX1, Am. J. Med. Genet. A 161a (2013) 803–808.

[17] M. Reichert, S. Takano, J. von Burstin, S.B. Kim, J.S. Lee, K. Ihida-Stansbury, C. Hahn, S. Heeg, G. Schneider, A.D. Rhim, B.Z. Stanger, A.K. Rustgi, The Prrx1 homeodomain transcription factor plays a central role in pancreatic regeneration and carcinogenesis, Genes Dev. 27 (2013) 288–300.

[18] S. Takano, M. Reichert, B. Bakir, K.K. Das, T. Nishida, M. Miyazaki, S. Heeg, M.A. Collins, B. Marchand, P.D. Hicks, A. Maitra, A.K. Rustgi, Prrx1 isoform switching regulates pancreatic cancer invasion and metastatic colonization, Genes Dev. 30 (2016) 233–247.

[19] M. Sugiyama, H. Hasegawa, S. Ito, K. Sugiyama, M. Maeda, K. Aoki, T. Wakabayashi, M. Hamaguchi, A. Natsume, T. Senga, Paired related homeobox 1 is associated with the invasive properties of glioblastoma cells, Oncol. Rep. 33 (2015) 1123–1130.

[20] O.H. Ocana, R. Corcoles, A. Fabra, G. Moreno-Bueno, H. Acloque, S. Vega, A. Barrallo-Gimeno, A. Cano, M.A. Nieto, Metastatic colonization requires the repression of the epithelial-mesenchymal transition inducer Prrx1, Cancer Cell 22 (2012) 709–724.

[21] H. Zhu, G. Sun, Loss of PRRX1 induces epithelial-mesenchymal transition and cancer stem cell-like properties in A549 cells, Am. J. Transl. Res. 9 (2017) 1641–1650.

[22] H. Hirata, K. Sugimachi, Y. Takahashi, M. Ueda, S. Sakimura, R. Uchi, J. Kurashige, Y. Takano, S. Nanbara, H. Komatsu, T. Saito, Y. Shinden, T. Iguchi, H. Eguchi, K. Atsumi, K. Sakamoto, T. Doi, M. Hirakawa, H. Honda, K. Mimori, Downregulation of PRRX1 confers cancer stem cell-like properties and predicts poor prognosis in hepatocellular carcinoma, Ann. Surg. Oncol. 22 (Suppl 3) (2015) S1402–S1409.

[23] A.J. Mutsaers, C.R. Walkley, Cells of origin in osteosarcoma: mesenchymal stem cells or osteoblast committed cells? Bone 62 (2014) 56–63.

[24] P.P. Lin, M.K. Pandey, F. Jin, A.K. Raymond, H. Akiyama, G. Lozano, Targeted mutation of p53 and Rb in mesenchymal cells of the limb bud produces sarcomas in mice, Carcinogenesis 30 (2009) 1789–1795.

[25] S.D. Berman, E. Calo, A.S. Landman, P.S. Danielian, E.S. Miller, J.C. West, B.D. Fonhoue, A. Caron, R. Bronson, M.L. Bouxsein, S. Mukherjee, J.A. Lees, Metastatic osteosarcoma induced by inactivation of Rb and p53 in the osteoblast lineage, Proc. Natl. Acad. Sci. U.S.A. 105 (2008) 11851–11856.

[26] T. Quist, H. Jin, J.F. Zhu, K. Smith-Fry, M.R. Capecchi, K.B. Jones, The impact of osteoblastic differentiation on osteosarcomagenesis in the mouse, Oncogene 34 (2015) 4278–4284.

[27] K. Yan, J. Gao, T. Yang, Q. Ma, X. Qiu, Q. Fan, B. Ma, MicroRNA-34a inhibits the proliferation and metastasis of osteosarcoma cells both *in vitro* and *in vivo*, PLoS ONE 7 (2012) e33778.

[28] O. Ben-Izhak, Z. Laster, S. Araidy, R.M. Nagler, TUNEL - an efficient prognosis predictor of salivary malignancies, Br. J. Cancer 96 (2007) 1101–1106.

[29] H.H. Luu, Q. Kang, J.K. Park, W. Si, Q. Luo, W. Jiang, H. Yin, A.G. Montag, M.A. Simon, T.D. Peabody, R.C. Haydon, C.W. Rinker-Schaeffer, T.C. He, An orthotopic model of human osteosarcoma growth and spontaneous pulmonary metastasis, Clin. Exp. Metastasis 22 (2005) 319–329.

[30] H.C. Graat, M.A. Witlox, F.H. Schagen, G.J. Kaspers, M.N. Helder, J. Bras, G.R. Schaap, W.R. Gerritsen, P.I. Wuisman, V.W. van Beusechem, Different susceptibility of osteosarcoma cell lines and primary cells to treatment with oncolytic adenovirus and doxorubicin or cisplatin, Br. J. Cancer 94 (2006) 1837–1844.

[31] H. Jiang, H.C. Reinhardt, J. Bartkova, J. Tommiska, C. Blomqvist, H. Nevanlinna, J. Bartek, M.B. Yaffe, M.T. Hemann, The combined status of ATM and p53 link tumor development with therapeutic response, Genes Dev. 23 (2009) 1895–1909.

[32] M. van der Deen, H. Taipaleenmaki, Y. Zhang, N.M. Teplyuk, A. Gupta, S. Cinghu, K. Shogren, A. Maran, M.J. Yaszemski, L. Ling, S.M. Cool, D.T. Leong, C. Dierkes, J. Zustin, M. Salto-Tellez, Y. Ito, S.C. Bae, M. Zielenska, J.A. Squire, J.B. Lian, J.L. Stein, G.P. Zambetti, S.N. Jones, M. Galindo, E. Hesse, G.S. Stein, A.J. van Wijnen, MicroRNA-34c inversely couples the biological functions of the runt-related transcription factor RUNX2 and the tumor suppressor p53 in osteosarcoma, J. Biol. Chem. 288 (2013) 21307–21319.

[33] J. Lamb, E.D. Crawford, D. Peck, J.W. Modell, I.C. Blat, M.J. Wrobel, J. Lerner, J.P. Brunet, A. Subramanian, K.N. Ross, M. Reich, H. Hieronymus, G. Wei, S.A. Armstrong, S.J. Haggarty, P.A. Clemons, R. Wei, S.A. Carr, E.S. Lander, T.R. Golub, The connectivity map: using gene-expression signatures to connect small molecules, genes, and disease, Science 313 (2006) 1929–1935.

[34] A.M. Brum, J. van de Peppel, C.S. van der Leije, M. Schreuders-Koedam, M. Eijken, B.C. van der Eerden, J.P. van Leeuwen, Connectivity map-based discovery of parbendazole reveals targetable human osteogenic pathway, Proc. Natl. Acad. Sci. U.S.A. 112 (2015) 12711–12716.

[35] A. Subramanian, R. Narayan, S.M. Corsello, D.D. Peck, T.E. Natoli, X. Lu, J. Gould, J.F. Davis, A.A. Tubelli, J.K. Asiedu, D.L. Lahr, J.E. Hirschman, Z. Liu, M. Donahue, B. Julian, M. Khan, D. Wadden, I.C. Smith, D. Lam, A. Liberzon, C. Toder, M. Bagul, M. Orzechowski, O.M. Enache, F. Piccioni, S.A. Johnson, N.J. Lyons, A.H. Berger, A.F. Shamji, A.N. Brooks, A. Vrcic, C. Flynn, J. Rosains, D.Y. Takeda, R. Hu, D. Davison, J. Lamb, K. Ardlie, L. Hogstrom, P. Greenside, N.S. Gray, P.A. Clemons, S. Silver, X. Wu, W.N. Zhao, W. Read-Button, X. Wu, S.J. Haggarty, L.V. Ronco, J.S. Boehm, S.L. Schreiber, J.G. Doench, J.A. Bittker, D.E. Root, B. Wong, T.R. Golub, A next generation connectivity map: L1000 platform and the first 1,000,000 profiles, Cell 171 (2017) 1437–1452 e1417.

[36] M. Logan, J.F. Martin, A. Nagy, C. Lobe, E.N. Olson, C.J. Tabin, Expression of Cre recombinase in the developing mouse limb bud driven by a Prxl enhancer, Genesis 33 (2002) 77–80.

[37] H. Akiyama, J.E. Kim, K. Nakashima, G. Balmes, N. Iwai, J.M. Deng, Z. Zhang, J.F. Martin, R.R. Behringer, T. Nakamura, B. de Crombrugghe, Osteo-chondroprogenitor cells are derived from Sox9 expressing precursors, Proc. Natl. Acad. Sci. U.S.A. 102 (2005) 14665–14670.

[38] L.T.H. Phi, I.N. Sari, Y.G. Yang, S.H. Lee, N. Jun, K.S. Kim, Y.K. Lee, H.Y. Kwon, Cancer stem cells (CSCs) in drug resistance and their therapeutic implications in cancer treatment, Stem Cells Int. 2018 (2018) 5416923.

[39] K. Shimozaki, G.D. Clemenson Jr., F.H. Gage, Paired related homeobox protein 1 is a regulator of stemness in adult neural stem/progenitor cells, J. Neurosci. 33 (2013) 4066–4075.

[40] J. Dong, Z. Lv, Q. Chen, X. Wang, F. Li, PRRX1 drives tamoxifen therapy resistance through induction of epithelial-mesenchymal transition in MCF-7 breast cancer cells, Int. J. Clin. Exp. Pathol. 11 (2018) 2629–2635.

[41] J. Guo, Z. Fu, J. Wei, W. Lu, J. Feng, S. Zhang, PRRX1 promotes epithelial-mesenchymal transition through the Wnt/β-catenin pathway in gastric cancer, Med. Oncol. 32 (2015) 393.

[42] Y. Takahashi, G. Sawada, J. Kurashige, R. Uchi, T. Matsumura, H. Ueo, Y. Takano, S. Akiyoshi, H. Eguchi, T. Sudo, K. Sugimachi, Y. Doki, M. Mori, K. Mimori, Paired related homoeobox 1, a new EMT inducer, is involved in metastasis and poor prognosis in colorectal cancer, Br. J. Cancer 109 (2013) 307–311.

[43] W.P. Roos, A.D. Thomas, B. Kaina, DNA damage and the balance between survival and death in cancer biology, Nat. Rev. Cancer 16 (2016) 20–33.

[44] N.J. Curtin, DNA repair dysregulation from cancer driver to therapeutic target, Nat. Rev. Cancer 12 (2012) 801–817.

[45] M. Nagahashi, A. Yamada, E. Katsuta, T. Aoyagi, W.C. Huang, K.P. Terracina, N.C. Hait, J.C. Allegood, J. Tsuchida, K. Yuza, M. Nakajima, M. Abe, K. Sakimura, S. Milstien, T. Wakai, S. Spiegel, K. Takabe, Targeting the SphK1/S1P/S1PR1 axis that links obesity, chronic inflammation, and breast cancer metastasis, Cancer Res. 78 (2018) 1713–1725.

[46] X. You, Y. Wang, J. Wu, Q. Liu, D. Chen, D. Tang, D. Wang, Galectin-1 promotes metastasis in gastric cancer through a sphingosine-1-phosphate receptor 1-dependent mechanism, Cell. Physiol. Biochem. 51 (2018) 11–30.

[47] Q. Lin, L. Ren, M. Jian, P. Xu, J. Li, P. Zheng, Q. Feng, L. Yang, M. Ji, Y. Wei, J. Xu, The mechanism of the premetastatic niche facilitating colorectal cancer liver metastasis generated from myeloid-derived suppressor cells induced by the S1PR1-STAT3 signaling pathway, Cell Death Dis. 10 (2019) 693.